Single Particle SEM-EDX Analysis of Iron-Containing Coarse Particulate Matter in an Urban Environment: Sources and Distribution of Iron within Cleveland, Ohio

Andrew P. Ault,[1] Thomas M. Peters,[2]* Eric J. Sawvel,[2] Gary S. Casuccio,[3] Robert D. Willis,[4] Gary A. Norris,[4] and Vicki H. Grassian[1]*

[1] Department of Chemistry, University of Iowa, Iowa City, Iowa, 52242

[2] Department of Occupational and Environmental Health, University of Iowa, Iowa City, Iowa, 52242

[3] RJ Lee Group, Inc., Monroeville, Pennsylvania, 15146

[4] United States Environmental Protection Agency, Office of Research and Development, Research Triangle Park, North Carolina 27711

*corresponding authors e-mails: thomas-m-peters@uiowa.edu and vicki-grassian@uiowa.edu

Abstract

The physicochemical properties of coarse-mode, iron-containing particles, and their temporal and spatial distributions are poorly understood. Single particle analysis combining x-ray elemental mapping and computer-controlled scanning electron microscopy (CCSEM-EDX) of passively collected particles was used to investigate the physicochemical properties of iron-containing particles in Cleveland, Ohio in summer 2008 (Aug.-Sept.), summer 2009 (Jul.-Aug.), and winter 2010 (Feb.-Mar.). The most abundant classes of iron-containing particles were mineral dust, iron oxide fly ash, NaCl containing agglomerates (likely from road salt), and Ca-S containing agglomerates (likely from slag, a byproduct of steel production, or gypsum in road salt). The mass concentrations of anthropogenic fly ash particles were highest in the Flats region (downtown) and decreased with distance away from this region. The concentrations of fly ash in the Flats region were consistent with inter-annual changes in steel production. These particles were observed to be highly spherical in the Flats region, but less so after transport away from downtown. This change in morphology may be attributed to atmospheric processing. Overall, this work demonstrates that the method of passive collection with single particle analysis by electron microscopy is a powerful tool to study spatial and temporal gradients in components of coarse particles. These gradients may correlate with human health effects associated with exposure to coarse-mode PM.

Introduction

Ambient particulate matter (PM) has been associated with negative impacts on human health, including adverse respiratory, cardiovascular, and cardiopulmonary health outcomes.[1-3] While the effects of fine PM, $PM_{2.5}$ (PM < 2.5 μm, aerodynamic diameter) have long been established,[3] coarse PM, $PM_{10\text{-}2.5}$, (10 μm > PM > 2.5 μm, aerodynamic diameter) has recently received greater attention.[4] Positive associations have been observed between $PM_{10\text{-}2.5}$ and a variety of health problems including cardiovascular diseases,[5] mortality,[6] asthma,[7] respiratory diseases,[8] and chronic obstructive pulmonary disease (COPD).[4] Knowledge of the chemical species in $PM_{10\text{-}2.5}$ is needed to better understand these health effects and to identify sources for possible regulatory action.

Transition metals in PM have been identified as potentially important contributors to biological responses that lead to adverse health effects.[9] Iron is the most abundant transition metal in the atmosphere[10] that may either be lofted into the atmosphere as wind-blown mineral dust or emitted as a byproduct of combustion processes (e.g. coal combustion), steelworks, and other industrial sources.[10,11] Iron particles from combustion can represent more than 50% of the total iron deposited in areas near combustion sources[12] and at remote sites.[13] Iron in particles from combustion processes is more soluble than iron in mineral dust and therefore thought to be more bioavailable,[12] which could have important health implications. The chemical form of iron, and thus bioavailability, of natural mineral dust vs. anthropogenic combustion is being studied from both chemical[14,15] and biogeochemical perspectives.[16]

Given its abundance in the atmosphere, the health effects of iron have been investigated in a number of studies.[17-19] Ghio and Devlin showed that PM emitted from a steel mill adversely impacted pulmonary health greater than a similar amount of PM from the same area when the mill was not in production, attributable to metals including iron.[18] Carter et al. showed that iron (as well as vanadium and nickel) increased cytokine production in human airway epithelial cells.[19] Wei et al. reported that PM containing iron increased reactive oxygen species (ROS), activated NF-κB, and led to cell death.[17] Verma et al. found that iron in diesel exhaust particles explained 84% of the variance in ROS produced by an in vitro macrophage-based assay.[20] Iron-rich particles from Saharan dust storms have been associated with increased daily mortality in Spain.[21]

New sampling and analysis methods are available to study the inter-annual and spatial variability in the physicochemical properties of metal-containing coarse particles. Since concentrations of coarse particles have spatial distributions that are often highly heterogeneous due to their shorter atmospheric lifetimes compared to fine particles,[5] it is important to determine their spatial variability and changes in their physicochemical properties. Passive samplers are a low cost, energy efficient method to collect multiple samples simultaneously in different locations.[22-25] Mass concentrations determined with passive samplers have demonstrated strong correlation with dichotomous samplers,[22] and are increasingly being used to investigate spatial variability of $PM_{10-2.5}$ in urban areas.[26,27] Recently, improved microscopy and spectroscopy methods have been applied to iron-containing particles, including: scanning electron microscopy (SEM),[28] micro-focused X-ray absorption spectroscopy (μ-XAS),[29] micro-focused X-ray diffraction (μ-XRD),[29,30] and micro-X-ray absorption near edge spectroscopy (μ-XANES).[30,31]

In this study, we investigate the concentration, chemical composition and physical properties of iron-containing particles passively sampled in the Cleveland, Ohio air shed, using single particle electron microscopy. Of particular interest is the heterogeneous chemistry of combustion-generated iron-containing particles (referred to hereafter as fly ash), which has the potential to lead to higher concentrations of bioavailable iron upon inhalation and could lead to adverse health effects.[32] The spatial distribution and concentration of fly ash particles followed trends in emissions from anthropogenic sources. These particles were also found to evolve as they move away from their source. Given the spatial and interannual variation in sources and concentrations, efforts to improve the exposure assessments spatially within urban areas are necessary to avoid potential misidentification of underlying causes for negative health effects due to particulate matter.

Experimental Methods

Cleveland Sampling Sites. Sampling of $PM_{10-2.5}$ was conducted in Cleveland, Ohio in summer 2008, summer 2009, and winter 2010 as part of the Environmental Protections Agency's Cleveland Multiple Air Pollutants Study (CMAPS) (http://www.rtord.epa.gov/ordfactsheets/index.cfm?fuseaction=home.FactSheetDetail&FactSheetID=460). Sampling sites were distributed across the Cleveland metropolitan area from the industrial Flats region adjacent to downtown out to suburban Medina (~33 miles southwest of downtown). Twenty-five sites were chosen for the 2008 study based on a satellite-based remote sensing method to design spatial sampling for intra-urban population exposure assessment,[33] which was applied to the Cleveland area.[34] Different monitoring sites were used for the 2009 and

2010 studies, although there was some overlap with the 2008 sites. The process used to select sites is described by Mukerjee et al.,[35] and was based on a land-use regression (LUR) modeling study. The selection of these sites was based on the need to span the mathematical space determined by the model's explanatory variables (e.g., traffic intensity, distance to roadways, and other urban land-use variables).

Samples were collected on polycarbonate substrates inside a passive sampler housing designed to minimize the effects of wind and precipitation.[36] Seven-day samples were collected each week for three weeks in 2008 (August 12- September 2), five weeks in 2009 (July 27 – August 29), and five weeks in 2010 (February 1 – March 9). This region experienced an economic downturn in late 2008 (after our measurements were complete) that led to extensive industrial site closures in 2009 followed by the reopening of some sites in 2010. In 2009, lower industrial emissions resulted from no steel production during the sampling period, while in 2010 5,000 tons of steel were produced daily.[37] 2008 emissions inventory data is similar to 2010.[37,38] For the duration of the winter 2010 study, snow cover, which has been shown to suppress dust emission,[39-42] was prevalent across the region,[43] increasing with further distance from downtown.

Computer-Controlled Scanning Electron Microscopy Analysis. Substrates were analyzed by computer-controlled SEM (CCSEM) measurements with a Personal SEM®.[44,45] For 2008, 2009, and 2010 the number of particles analyzed each year was 29,331, 49,329, and 53,105, respectively. This automated analysis captured single particle physical properties, including: average diameter (d_{ave}), maximum diameter (d_{max}), minimum diameter (d_{min}), circular diameter (d_{circ}), projected area, and perimeter. Although particles across all size ranges up to

122 approximately 150 μm in diameter can deposit on the passive sampler, the CCSEM analysis for
123 these samples was confined only to particles satisfying 1.0 μm < d_a < 10 μm (d_a is aerodynamic
124 diameter), in order to capture the supermicron PM fraction. The process for converting to mass
125 concentration is described in detail in Wagner and Leith[23] and Ott et al.[22] Briefly, aerodynamic
126 diameter and particle mass are calculated from projected area diameter through the use of a
127 volumetric shape factor, aerodynamic shape factor, and particle density from tables for specified
128 oxides based on chemical composition.[22] Particle mass loading on the sample was converted to
129 ambient mass concentration using an empirically-derived deposition velocity model.[23,24] Further
130 details on the calculation of mass concentration from SEM data are given in Supporting
131 Information. Energy dispersive x-ray spectrometry (EDX) was used to determine the elemental
132 composition of individual particles. EDX spectra from individual particles were analyzed using a
133 vector based algorithm to determine the relative abundance of 19 elements: carbon (C), sodium
134 (Na), magnesium (Mg), aluminum (Al), silicon (Si), phosphorus (P), sulfur (S), chlorine (Cl),
135 potassium (K), calcium (Ca), titanium (Ti), chromium (Cr), manganese (Mn), iron (Fe), nickel
136 (Ni), copper (Cu), zinc (Zn), barium (Ba), and lead (Pb).[44] Iron-containing particles are defined
137 as those with a K-α peak at 6.4 keV representing greater than 2% of the quantified elemental
138 composition.
139
140 *Data Analysis.* Single particle data from the CCSEM-EDX analysis were imported into
141 MATLAB R2010a (MathWorks, Inc.) for analysis. Particles were analyzed through queries on
142 particle composition (Fe > 2%) and clustering using the k-means algorithm in the MATLAB
143 toolbox.[46,47] Clustering algorithms have been applied to CCSEM-EDX data for over 20 years,
144 with the most commonly used algorithm being adaptive resonance theory 2a (ART2a).[27,48] In

145 more recent years, the use of clustering for real-time single-particle mass spectrometry analysis
146 has shown that k-means is as effective as ART2a and is considerably simpler and faster to run.[49]
147 Further discussion of the application of clustering and error reduction is given in the Supporting
148 Information. After clustering, clusters were grouped into the basic classes based on mathematical
149 similarity, elemental composition and comparison with the literature, discussed below.
150
151 **Results and Discussion**
152 *Particles Containing Iron.* The mass concentration by size of all particles, iron-containing
153 particles, and the fraction of iron-containing particles per year are shown in Figure 1. (See
154 Sawvel et al.[50] for detailed analysis of all coarse particle mass, including the seasonal and
155 interannual variability of major particle classes). The mass concentration of all particles and iron-
156 containing particles were very similar in summer 2008 and summer 2009. In winter 2010, the
157 mass concentration of all particles was shifted to slightly larger particle sizes potentially due to a
158 large contribution of NaCl particles from application of road salt across the region. The fraction
159 of particles containing iron (blue line) was higher in summer 2008 and 2009 compared to winter
160 2010, when road salt was a large fraction of $PM_{10-2.5}$. Figure 1 shows that iron-containing
161 particles contribute substantially to coarse PM. However, the chemical composition and
162 properties of the iron-containing particles differ to a greater degree than is implied from the mass
163 concentrations and fractions, as discussed below.
164
165 *Major Classes of Iron-Containing Particles*. The iron-containing particles were categorized into
166 the following classes: fly ash, mineral dust, NaCl agglomerates, and Ca-S agglomerates. Figure 2
167 shows the average EDX spectrum and digital color histogram for each of the four major classes

168 of iron-containing particles. The digital color histogram shows the fraction of particles in that
169 class containing a specific element, while the color represents the fraction of particles whose
170 peak intensity falls in that range. For example, 96% of particles in the mineral dust class contain
171 silicon and 19% of all mineral dust particles have silicon peaks comprising 30-50% (red block)
172 of the normalized x-ray counts for an individual particle. Although carbon was measured with
173 CCSEM-EDX, it is difficult, especially for smaller particles, to determine how much of the
174 carbon signal comes from the particle and how much is generated from the underlying
175 polycarbonate substrate. For this reason, carbon was not used in determining particle
176 classification. The number of particles from each class for each year is reported in Table S1 of
177 the Supporting Information.
178
179 SEM images of representative particles for the different particle classes observed are shown in
180 Figure 3 (Column 1). Columns 2-6 show EDX elemental maps of Fe, O, Al-Si, and Na-Ca to
181 identify the distribution of the different elements within representative particles. For some
182 particles with high X-ray emission, particles appeared to contain a marker in the elemental map
183 that was not present in the EDX spectra (i.e. Al-Si in fly ash particles). This is a common
184 problem in EDX elemental mapping[51] and samples where there was no evidence of a specific
185 marker in the EDX spectrum are labeled "No Signal In Spectrum" in Figure 3. Particles
186 containing iron that did not fit into one of these five classes are not discussed in detail as they
187 had highly varying composition and represented less than 1% of the $PM_{10-2.5}$ mass concentration.
188
189 The fly ash class was characterized by particles that contained mostly iron (Figure 2a). These
190 particles were quite spherical (Figure 3a) and contained an even distribution of iron and oxygen

191 throughout (oxygen was only identified through SEM-EDX mapping), which agrees with
192 previous measurements of fly ash particles emitted from steel facilities.[52,53] The spherical shape
193 is due to the molten nature of the material at high temperatures when the particles are formed
194 during steel production or other industrial processes.[54] Due to their high iron (and low aluminum
195 and silicon) content, these particles are attributed to fly ash from high temperature processes in
196 steel production, though a small fraction may be from power generation or other industrial
197 sources within the air shed.
198
199 Mineral dust particles were characterized by high fractions and intensities of aluminum and
200 silicon, likely in the form of aluminosilicates, along with other crustal elements including
201 magnesium, calcium, potassium, and iron (Figure 2b).[55,56] The mineral dust class showed a great
202 deal of variability in composition, and the class shown here represents a combination of four
203 different clusters: silicate dust, aluminosilicate dust, calcium-rich dust, and titanium-rich dust. In
204 contrast to the fly ash particles (Figure 3a), the mineral dust particles displayed an irregular and
205 rough morphology (Figure 3b) due to a mixture of different mineral crystals within a single
206 particle. The elemental maps for mineral dust show a heterogeneous distribution of different
207 minerals within individual particles.[57] Mineral dust makes up the largest fraction of global
208 aerosol mass in the atmosphere[58] and can be lofted into the air by wind[59] and by vehicles on
209 roadways.[60,61]
210
211
212 These major iron-containing classes (mineral dust and fly ash) were observed to be mixed with
213 NaCl and Ca-S as agglomerates (Figures 2c and 2d). The NaCl agglomerate class contained

214 particles that were frequently cube-shaped with small iron inclusions or iron flakes (Figure 3c).
215 Na and Cl (Cl not shown) were evenly distributed throughout these particles. $PM_{10-2.5}$ was
216 highest in winter 2010 probably due to NaCl from road salt either from dry resuspension or
217 resuspension of salt spray from cars traveling on wet roads. These particles were not present in
218 summer 2008 or summer 2009. Road salt is used commonly to improve road conditions in the
219 winter season and has been shown to impact urban PM.[27,62] The particles that compose the Ca-S
220 agglomerate class fall into two categories. The particle shown in Figure 3d is an example of a
221 Ca-S type particle that is an agglomerate with a mineral dust particle. Ca and S are markers for
222 slag and cement production, as has been shown elsewhere.[63] Though less frequent, a Ca-S-O
223 containing agglomerate (most likely gypsum - $CaSO_4$) was observed as well (as in Figure 3c)
224 associated with aqueous droplets containing NaCl particles, likely gypsum from road salt. Ca-S
225 agglomerates were not observed in 2008 and 2009. Elemental mapping was valuable in
226 confirming the two primary forms of iron-containing particles: mineral dust and fly ash, and in
227 identifying agglomerates of the primary iron-containing particles with abundant non-iron-
228 containing classes.
229
230 *Circularity and Aspect Ratio of the Different Major Classes.* Particles in each of the four main
231 classes and the "Other" category were binned according to circularity (C) and aspect ratio (AR),
232 equations 1 and 2, respectively:

$$C = 4\pi \frac{A}{P^2} \quad (1)$$

$$AR = \frac{d_{max}}{d_{perp}} \quad (2)$$

where A = area of the particle, P = perimeter of the particle, d_{max} is the maximum diameter of the particle and d_{perp} is the diameter perpendicular to d_{max}. The normalized circularity and aspect ratio (binned logarithmically to highlight values close to unity) for each year are shown in Figure 4. Circularity of 1 indicates a particle that is perfectly spherical, while an aspect ratio of 1 denotes a particle that is not elongated in any direction. The particles in the fly ash class had the highest circularities and the lowest aspect ratios, as would be expected for spherical particles. Interestingly, during the steel industry shutdown in 2009, the average circularity of the fly ash class of particles decreased compared to 2008 and 2010. A possible explanation is that the fly ash class of 2009 came from other sources (sources not emitting spherical particles) or comprises particles that have undergone heterogeneous reactions which break down the particle and decrease particle sphericity,[32] or adsorption of secondary species with less than complete surface coverage leading to increased surface roughness and reduced sphericity (see Figure S2 in Supporting Information).

The mineral dust and particle class, observed in all three years, showed consistent, non-spherical circularity and aspect ratio distributions (Figure 4). The NaCl and Ca-S agglomerates were only observed in 2010 and were both quite non-spherical as well, though the NaCl agglomerate may have been aqueous and thus spherical prior to loss of water on the substrate or in the SEM. It should be noted that if any of these particles were in the aqueous phase and solidified under the vacuum of the SEM they may appear less spherical than they were when present in the atmosphere.

255 *Mass Distributions of the Five Major Classes*. Figure 5 shows stacked mass size distributions for
256 the main particle classes averaged across all sites for each sampling year (column 1), averaged
257 for sites in the Cleveland Flats where industrial sources are concentrated (column 2), averaged
258 for the rest of Cleveland (column 3), and averaged for the rural background site at Medina
259 (column 4). Additionally, the mass size distribution for all particles is shown (black line) to
260 provide context as to the contribution of iron-containing particles to the coarse mass
261 concentration in each region. As Medina was not used in 2008 a map of the sites across the
262 Cleveland area is shown. Previous studies have shown maps of the Cleveland area and sources,[64]
263 as well as sites used for the CMAP studies.[34,50] The mineral dust concentrations in 2008 and
264 2009 were quite similar, as were their percentage of total coarse mass (21 and 17%,
265 respectively), indicating inter-annual consistency in background mineral dust concentrations in
266 summer. The lower concentrations observed in winter are likely due to the snow cover[43]
267 reducing wind-blown suspension of mineral dust.[39-42] Models have predicted lower windblown
268 dust emissions for Cleveland in winter, while anthropogenic fugitive dusts are predicted to be
269 constant year round under typical conditions.[65] The mass concentration of fly ash particles and
270 percent of iron-containing mass was notably lower in 2009 (12%) than in 2008 (28%) or 2010
271 (32%), consistent with the shutdown of steel production facilities in 2009. During this shutdown,
272 fly ash concentrations decreased across all sites, most notably in the Flats, but also in the rest of
273 Cleveland. If, as seems likely, these decreases were in response to the temporary shutdown of the
274 steel facilities, then the data in Figure 5 show that the potential for exposure to iron-containing
275 emissions from sources in the Flats extends across the entire Cleveland metropolitan area.
276

277 The mass concentration of all classes of iron-containing particles decreased with increasing
278 distance from the Flats (Figure 5, columns 2-4). The decrease was similar for fly ash particles in
279 summer 2008 and winter 2010, but less dramatic in summer 2009. The reduced spatial gradient
280 in 2009 is again likely due to the shutdown of emission sources in the Flats for that year.
281
282 Similar spatial patterns were observed for mineral dust particles with decreasing concentrations
283 with increasing distance away from the Flats. (Medina was not sampled in 2008). In summer
284 2009 (during the economic downturn), this decrease was smaller for both total and iron-
285 containing particle concentrations. In winter 2010, substantial mineral dust concentrations were
286 observed in the Flats, although they were quite low at Medina. The rural nature of the Medina
287 site may lead to a greater fraction of snow cover that likely suppresses wind-blown dust, whereas
288 the high volume of industry and road activity may lead to significant concentrations of re-
289 suspended road dust in the Flats even in winter. Consequently, we attribute mineral dust in
290 winter to anthropogenic influences, whereas mineral dust in the summer of 2009, during a period
291 of reduced industrial output is attributed to naturally occurring wind-blown resuspension. The
292 highest mineral dust concentrations (summer 2008 in the Flats) are attributed to a combination of
293 anthropogenic sources of mineral dust (road dust and industry) and naturally occurring dust. The
294 concentration of NaCl agglomerates was also highest in the Flats, where there is a high volume
295 of vehicular traffic and road salt dispersal combined with a high concentration of iron-containing
296 particles. Ca-S agglomerates were also highest in the Flats consistent with the close vicinity of
297 steel and cement production.
298

299 *Processing of Fly Ash Particles during Atmospheric Transport*. The findings in this study
300 suggest that fly ash particles react and lose sphericity during transport away from their
301 predominant source in the Flats, a contrast to increases in sphericity that are observed for
302 submicron particles with high sulfur content.[66] The circularities of fly ash particles were grouped
303 by location, binned, and normalized for 2008 and 2010 when there was significant steel
304 production in the Flats (Figure 6). More than 26 ± 1% of the fly ash particles were near-perfect
305 spheres (circularity > 0.95) in the Flats, compared to less than 11 ± 1% away from the Flats, with
306 circularity distributions peaking at 0.80 in 2008 and 0.83 in 2010. The particles at Medina in
307 2010 have a similar distribution to the rest of Cleveland and are significantly less spherical than
308 fly ash in the Flats region (7 ± 2 % in spherical bin), which suggests that the particles have likely
309 already aged or were emitted from different sources that produce less spherical particles. The
310 circularities of the other particle classes did not change appreciably with distance from the Flats
311 (not shown). Taken together, the spatially resolved circularity data indicate that fly ash particles
312 most likely either react with inorganic acids (i.e. sulfuric acid) causing their spherical shape to
313 degrade or take up secondary species in a non-uniform manner during transport to downwind
314 locations across the metropolitan area. Figure S2 in the Supporting Information shows a particle
315 that may have undergone processes leading to a decrease in sphericity. Changes to fly ash
316 chemical and physical properties due to such reactions have been demonstrated in recent
317 laboratory studies.[67]
318
319 **Atmospheric Implications**
320 The two-season Cleveland study provided a unique opportunity to characterize coarse PM over a
321 three year time period during which a major industrial activity was shut down. Iron-containing

322 particles from natural and anthropogenic sources were found to represent a significant fraction of
323 total $PM_{10-2.5}$ in the Cleveland air shed. The importance of anthropogenic iron-containing
324 particles in the atmosphere has been highlighted in recent years, particularly as soluble iron
325 concentrations have exceeded estimates based solely on mineral dust aerosol.[12] Determining
326 sources of iron-containing particles and understanding the distribution and evolution of these
327 particles across urban air sheds are critically important to better understand and predict adverse
328 health effects from exposure to PM. Herein, we have shown that industrial sources can be a
329 major source of iron-containing particles, particularly fly ash, across the Cleveland air shed. The
330 concentration of these particles decreases strongly with distance from source emissions. For
331 example, fly ash particles attributed to steel production were present in high concentrations in
332 2008 and 2010 in the industrial Flats region downtown and transported across the Cleveland
333 metropolitan area. These fly ash particles lose their spherical shape during transport to suburban
334 areas possibly due to heterogeneous reactions and secondary species condensation. Such
335 processes could potentially increase the amount of soluble, bioavailable iron en route.
336 Interestingly, even naturally occurring iron-containing mineral dust particles are suspended in the
337 atmosphere to a greater degree in areas with high vehicular traffic and industrial production. To
338 fully evaluate the health effects posed by iron-containing particles further studies are needed to
339 better understand the different types of iron-containing aerosols observed in highly populated
340 areas, their spatial and temporal variability, as well as the effect of heterogeneous reactions and
341 how these reactions may lead to more bioavailable iron that has the potential to lead to greater
342 negative health effects.
343
344 **Acknowledgments and Disclaimer**

345 The authors acknowledge the Central Microscopy Research Facility (CMRF) at the University of
346 Iowa for assistance with microscopy measurements. Thomas Rebotier and David Musicant are
347 acknowledged for useful conversations on clustering algorithms. The United States Environmental
348 Protection Agency through its Office of Research and Development funded and collaborated in the
349 research described here under contracts EP09D000463 and EP11D000010 to the University of
350 Iowa. It has been subjected to Agency review and approved for publication.
351

References

1. Brook, R. D.; Rajagopalan, S.; Pope, C. A.; Brook, J. R.; Bhatnagar, A.; Diez-Roux, A. V.; Holguin, F.; Hong, Y. L.; Luepker, R. V.; Mittleman, M. A.; Peters, A.; Siscovick, D.; Smith, S. C.; Whitsel, L.; Kaufman, J. D.; Amer Heart Assoc Council Epidemiol; Council Kidney Cardiovasc, D.; Council Nutr Phys Activity, M., Particulate Matter Air Pollution and Cardiovascular Disease An Update to the Scientific Statement From the American Heart Association. *Circulation* **2010,** *121*, (21), 2331-2378.
2. Pope, C. A., Mortality effects of longer term exposures to fine particulate air pollution: Review of recent epidemiological evidence. *Inhalation Toxicology* **2007,** *19*, 33-38.
3. Dockery, D. W.; Pope, C. A.; Xu, X. P.; Spengler, J. D.; Ware, J. H.; Fay, M. E.; Ferris, B. G.; Speizer, F. E., An association between air pollution and mortality in 6 United States Cities. *New England Journal of Medicine* **1993,** *329*, (24), 1753-1759.
4. Brunekreef, B.; Forsberg, B., Epidemiological evidence of effects of coarse airborne particles on health. *European Respiratory Journal* **2005,** *26*, (2), 309-318.
5. Chang, H. H.; Peng, R. D.; Dominici, F., Estimating the acute health effects of coarse particulate matter accounting for exposure measurement error. *Biostatistics* **2011,** *12*, (4), 637-52.
6. Malig, B. J.; Ostro, B. D., Coarse particles and mortality: evidence from a multi-city study in California. *Occupational And Environmental Medicine* **2009,** *66*, (12), 832-839.
7. Tecer, L. H.; Alagha, O.; Karaca, F.; Tuncel, G.; Eldes, N., Particulate matter (PM2.5, PM10-2.5, and PM10) and children's hospital admissions for asthma and respiratory diseases: A bidirectional case-crossover study. *Journal Of Toxicology And Environmental Health-Part A-Current Issues* **2008,** *71*, (8), 512-520.
8. Host, S.; Larrieu, S.; Pascal, L.; Blanchard, M.; Declercq, C.; Fabre, P.; Jusot, J. F.; Chardon, B.; Le Tertre, A.; Wagner, V.; Prouvost, H.; Lefranc, A., Short-term associations between fine and coarse particles and hospital admissions for cardiorespiratory diseases in six French cities. *Occupational And Environmental Medicine* **2008,** *65*, (8), 544-551.
9. Chen, L. C.; Lippmann, M., Effects of metals within ambient air particulate matter (PM) on human health. *Inhalation Toxicology* **2009,** *21*, (1), 1-31.
10. Deguillaume, L.; Leriche, M.; Desboeufs, K.; Mailhot, G.; George, C.; Chaumerliac, N., Transition Metals in Atmospheric Liquid Phases: Sources, Reactivity, and Sensitive Parameters. *Chemical Reviews* **2005,** *105*, (9), 3388-3431.
11. Mahowald, N. M.; Engelstaedter, S.; Luo, C.; Sealy, A.; Artaxo, P.; Benitez-Nelson, C.; Bonnet, S.; Chen, Y.; Chuang, P. Y.; Cohen, D. D.; Dulac, F.; Herut, B.; Johansen, A. M.; Kubilay, N.; Losno, R.; Maenhaut, W.; Paytan, A.; Prospero, J. A.; Shank, L. M.; Siefert, R. L., Atmospheric Iron Deposition: Global Distribution, Variability, and Human Perturbations. In *Annual Review of Marine Science*, 2009; Vol. 1, pp 245-278.
12. Luo, C.; Mahowald, N.; Bond, T.; Chuang, P. Y.; Artaxo, P.; Siefert, R.; Chen, Y.; Schauer, J., Combustion iron distribution and deposition. *Global Biogeochemical Cycles* **2008,** *22*, (1).
13. Furutani, H.; Jung, J.; Miura, K.; Takami, A.; Kato, S.; Kajii, Y.; Uematsu, M., Single-particle chemical characterization and source apportionment of iron-containing atmospheric aerosols in Asian outflow. *J. Geophys. Res.* **2011,** *116*, (D18), D18204.
14. Pehkonen, S. O.; Siefert, R.; Erel, Y.; Webb, S.; Hoffmann, M. R., Photoreduction of iron oxyhydroxides in the presence of important atmospheric organic-compounds. *Environmental Science & Technology* **1993,** *27*, (10), 2056-2062.
15. Takahashi, Y.; Higashi, M.; Furukawa, T.; Mitsunobu, S., Change of iron species and iron solubility in Asian dust during the long-range transport from western China to Japan. *Atmospheric Chemistry And Physics* **2011,** *11*, (21), 11237-11252.

16. Sedwick, P. N.; Sholkovitz, E. R.; Church, T. M., Impact of anthropogenic combustion emissions on the fractional solubility of aerosol iron: Evidence from the Sargasso Sea. *Geochemistry Geophysics Geosystems* **2007,** *8*.
17. Wei, H.; Wei, D.; Yi, S.; Zhang, F.; Ding, W., Oxidative stress induced by urban fine particles in cultured EA.hy926 cells. *Human & Experimental Toxicology* **2011,** *30*, (7), 579-590.
18. Ghio, A. J.; Devlin, R. B., Inflammatory lung injury after bronchial instillation of air pollution particles. *American Journal Of Respiratory And Critical Care Medicine* **2001,** *164*, (4), 704-708.
19. Carter, J. D.; Ghio, A. J.; Samet, J. M.; Devlin, R. B., Cytokine production by human airway epithelial cells after exposure to an air pollution particle is metal-dependent. *Toxicology And Applied Pharmacology* **1997,** *146*, (2), 180-188.
20. Verma, V.; Shafer, M. M.; Schauer, J. J.; Sioutas, C., Contribution of transition metals in the reactive oxygen species activity of PM emissions from retrofitted heavy-duty vehicles. *Atmospheric Environment* **2010,** *44*, (39), 5165-5173.
21. Perez, L.; Tobias, A.; Querol, X.; Kunzli, N.; Pey, J.; Alastuey, A.; Viana, M.; Valero, N.; Gonzalez-Cabre, M.; Sunyer, J., Coarse Particles From Saharan Dust and Daily Mortality. *Epidemiology* **2008,** *19*, (6), 800-807.
22. Ott, D. K.; Cyrs, W.; Peters, T. A., Passive measurement of coarse particulate matter, PM10-2.5. *Journal Of Aerosol Science* **2008,** *39*, (2), 156-167.
23. Wagner, J.; Leith, D., Passive aerosol sampler. Part I: Principle of operation. *Aerosol Science And Technology* **2001,** *34*, (2), 186-192.
24. Wagner, J.; Leith, D., Passive aerosol sampler. Part II: Wind tunnel experiments. *Aerosol Science And Technology* **2001,** *34*, (2), 193-201.
25. Yamamoto, N.; Hikono, M.; Koyama, H.; Kumagai, K.; Fujii, M.; Yanagisawa, Y., A passive sampler for airbome coarse particles. *Journal Of Aerosol Science* **2006,** *37*, (11), 1442-1454.
26. Ott, D. K.; Kumar, N.; Peters, T. M., Passive sampling to capture spatial variability in PM10-2.5. *Atmospheric Environment* **2008,** *42*, (4), 746-756.
27. Lagudu, U. R. K.; Raja, S.; Hopke, P. K.; Chalupa, D. C.; Utell, M. J.; Casuccio, G.; Lersch, T. L.; West, R. R., Heterogeneity of Coarse Particles in an Urban Area. *Environmental Science & Technology* **2011,** *45*, (8), 3288-3296.
28. Choel, M.; Deboudt, K.; Flament, P.; Aimoz, L.; Meriaux, X., Single-particle analysis of atmospheric aerosols at Cape Gris-Nez, English Channel: Influence of steel works on iron apportionment. *Atmospheric Environment* **2007,** *41*, (13), 2820-2830.
29. Elzinga, E. J.; Gao, Y.; Fitts, J. P.; Tappero, R., Iron speciation in urban dust. *Atmospheric Environment* **2011,** *45*, (26), 4528-4532.
30. Mayhew, L. E.; Webb, S. M.; Templeton, A. S., Microscale Imaging and Identification of Fe Speciation and Distribution during Fluid-Mineral Reactions under Highly Reducing Conditions. *Environmental Science & Technology* **2011,** *45*, (10), 4468-4474.
31. Oakes, M.; Weber, R. J.; Lai, B.; Russell, A. G.; Ingall, E. D., Characterization of iron speciation in single particles using XANES spectroscopy and micro X-ray fluorescence measurements: insight into factors controlling iron solubility. *Atmos. Chem. Phys. Discuss.* **2011,** *11*, 22771-22799.
32. Chen, H.; Laskin, A.; Baltrusaitis, J.; Gorski, C. A.; Scherer, M.; Grassian, V. H., Coal combustion fly ash as a source of iron in atmospheric dust. *Environmental Science & Technology* **2011,** *submitted.*
33. Kumar, N.; Nixon, V.; Sinha, K.; Jiang, X. S.; Ziegenhorn, S.; Peters, T., An Optimal Spatial Configuration of Sample Sites for Air Pollution Monitoring. *Journal Of The Air & Waste Management Association* **2009,** *59*, (11), 1308-1316.
34. Kumar, N.; Chu, A. D.; Foster, A. D.; Peters, T.; Willis, R., Satellite Remote Sensing for Developing Time and Space Resolved Estimates of Ambient Particulate in Cleveland, OH. *Aerosol Science And Technology* **2011,** *45*, (9), 1090-1108.

35. Mukerjee, S.; Smith, L. A.; Johnson, M. M.; Neas, L. M.; Stallings, C. A., Spatial analysis and land use regression of VOCs and NO(2) from school-based urban air monitoring in Detroit/Dearborn, USA. *Science Of The Total Environment* **2009,** *407*, (16), 4642-4651.
36. Ott, D. K.; Peters, T. M., A shelter to protect a passive sampler for coarse particulate matter, PM10-2.5. *Aerosol Science And Technology* **2008,** *42*, (4), 299-309.
37. Reid, B.; Pollard, E. K.; Du., Y.; Chinkin, L. R.; Hammond, D.; Norris, G. A. In *Development of a Local-Scale Emissions Inventory for the Cleveland Multiple Air Pollutant Study*, 19th Annual International Emission Inventory Conference "Emissions Inventories - Informing Emerging Issues, San Antonio, Texas, 2010; San Antonio, Texas, 2010.
38. EPA, 2008 National Emission Inventory Data. In 2008.
39. Tanaka, T. Y.; Sekiyama, T. T.; Maki, T.; Mikami, M., The Effects of Snow Cover and Soil Moisture on Asian Dust: I. A Numerical Sensitivity Study. *Sola* **2011,** *7A*, 36-39.
40. Sekiyama, T. T.; Tanaka, T. Y.; Maki, T.; Mikami, M., The Effects of Snow Cover and Soil Moisture on Asian Dust: II. Emission Estimation by Lidar Data Assimilation. *Sola* **2011,** *7A*, 40-43.
41. Laurent, B.; Marticorena, B.; Bergametti, G.; Mei, F., Modeling mineral dust emissions from Chinese and Mongolian deserts. *Global And Planetary Change* **2006,** *52*, (1-4), 121-141.
42. Shannon, S.; Lunt, D. J., A new dust cycle model with dynamic vegetation: LPJ-dust version 1.0. *Geoscientific Model Development* **2011,** *4*, (1), 85-105.
43. National Ice Center, NOAA: Snow Map Data Archive. In 2010.
44. Casuccio, G. S.; Schlaegle, S. F.; Lersch, T. L.; Huffman, G. P.; Chen, Y. Z.; Shah, N., Measurement of fine particulate matter using electron microscopy techniques. *Fuel Processing Technology* **2004,** *85*, (6-7), 763-779.
45. Casuccio, G. S.; Janocko, P. B.; Lee, R. J.; Kelly, J. F.; Dattner, S. L.; Mgebroff, J. S., The Use of Computer-Controlled Scanning Electron Electron Microscopy in Environmental Studies. *Journal Of The Air Pollution Control Association* **1983,** *33*, (10), 937-943.
46. Mucha, H. J., Späth, H.: Cluster dissection and analysis: theory, FORTRAN programs, examples. (Translator: Johannes Goldschmidt.) *Biometrical Journal* **1986,** *28*, (2), 182-182.
47. Seber, G. A. F., *Multivariate Observations*. John Wiley & Sons, Inc.: Hoboken, N. J., 1984.
48. Kim, D. S.; Hopke, P. K.; Massart, D. L.; Kaufman, L.; Casuccio, G. S., Multivariate Analysis of CCSEM Auto Emission Data. *Science Of The Total Environment* **1987,** *59*, 141-155.
49. Rebotier, T. P.; Prather, K. A., Aerosol time-of-flight mass spectrometry data analysis: A benchmark of clustering algorithms. *Analytica Chimica Acta* **2007,** *585*, (1), 38-54.
50. Sawvel, E. J.; Peters, T. M.; Kumar, N.; Casuccio, G. S.; Willis, R. D.; Hammond, D.; Norris, G. A.; Ault, A. P., Passive sampling to capture the spatial variability of coarse particles by composition in Cleveland, OH. *Atmospheric Environment* **2012,** *in prep.*
51. Friel, J. J.; Lyman, C. E., X-ray mapping in electron-beam instruments. *Microscopy and Microanalysis* **2006,** *12*, (1), 2-25.
52. Machemer, S. D., Characterization of airborne and bulk particulate from iron and steel manufacturing facilities. *Environmental Science & Technology* **2004,** *38*, (2), 381-389.
53. Choel, M.; Deboudt, K.; Flament, P., Development of Time-Resolved Description of Aerosol Properties at the Particle Scale During an Episode of Industrial Pollution Plume. *Water Air And Soil Pollution* **2010,** *209*, (1-4), 93-107.
54. Meyer, P. W. Spheroidal Beads from Boiler Slag and Fly Ash.
55. Sobanska, S.; Coeur, C.; Maenhaut, W.; Adams, F., SEM-EDX characterisation of tropospheric aerosols in the Negev desert (Israel). *Journal Of Atmospheric Chemistry* **2003,** *44*, (3), 299-322.
56. Coz, E.; Gomez-Moreno, F. J.; Pujadas, M.; Casuccio, G. S.; Lersch, T. L.; Artinano, B., Individual particle characteristics of North African dust under different long-range transport scenarios. *Atmospheric Environment* **2009,** *43*, (11), 1850-1863.
57. Conny, J. M.; Norris, G. A., Scanning Electron Microanalysis and Analytical Challenges of Mapping Elements in Urban Atmospheric Particles. *Environmental Science & Technology* **2011,** *45*, (17), 7380-7386.

58. Andreae, M. O.; Rosenfeld, D., Aerosol-cloud-precipitation interactions. Part 1. The nature and sources of cloud-active aerosols. *Earth-Sci. Rev.* **2008,** *89*, (1-2), 13-41.
59. Engelstaedter, S.; Tegen, I.; Washington, R., North African dust emissions and transport. *Earth-Sci. Rev.* **2006,** *79*, (1-2), 73-100.
60. Etyemezian, V.; Kuhns, H.; Gillies, J.; Chow, J.; Hendrickson, K.; McGown, M.; Pitchford, M., Vehicle-based road dust emission measurement (III): effect of speed, traffic volume, location, and season on PM10 road dust emissions in the Treasure Valley, ID. *Atmospheric Environment* **2003,** *37*, (32), 4583-4593.
61. Gehrig, R.; Hill, M.; Buchmann, B.; Imhof, D.; Weingartner, E.; Baltensperger, U., Separate determination of PM10 emission factors of road traffic for tailpipe emissions and emissions from abrasion and resuspension processes. *International Journal Of Environment And Pollution* **2004,** *22*, (3), 312-325.
62. Thornburg, J.; Rodes, C. E.; Lawless, P. A.; Williams, R., Spatial and temporal variability of outdoor coarse particulate matter mass concentrations measured with a new coarse particle sampler during the Detroit Exposure and Aerosol Research Study. *Atmospheric Environment* **2009,** *43*, (28), 4251-4258.
63. Khwaja, H. A.; Parekh, P. P.; Khan, A. R.; Hershey, D. L.; Naqvi, R. R.; Malik, A.; Khan, K., An In-Depth Characterization of Urban Aerosols Using Electron Microscopy and Energy Dispersive X-Ray Analysis. *Clean-Soil Air Water* **2009,** *37*, (7), 544-554.
64. Zhou, L.; Hopke, P. K.; Zhao, W. X., Source Apportionment of Airborne Particulate Matter for the Speciation Trends Network Site in Cleveland, OH. *Journal Of The Air & Waste Management Association* **2009,** *59*, (3), 321-331.
65. Park, S. H.; Gong, S. L.; Gong, W.; Makar, P. A.; Moran, M. D.; Zhang, J.; Stroud, C. A., Relative impact of windblown dust versus anthropogenic fugitive dust in PM(2.5) on air quality in North America. *Journal Of Geophysical Research-Atmospheres* **2010,** *115*.
66. Coz, E.; Artinano, B.; Robinson, A. L.; Casuccio, G. S.; Lersch, T. L.; Pandis, S. N., Individual particle morphology and acidity. *Aerosol Science And Technology* **2008,** *42*, (3), 224-232.
67. Chen, H.; Laskin, A.; Baltrusaitis, J.; Gorski, C. A.; Scherer, M. M.; Grassian, V. H., Coal Fly Ash as a Source of Iron in Atmospheric Dust. *Environmental Science & Technology* **2012,** *46*, (4), 2112-2120.

Figure Captions

Figure 1: Mass concentration by size of all particles (gray), iron-containing particles (red), and the fraction of iron-containing particles (blue line) in a) summer 2008, b) summer 2009, and c) winter 2010.

Figure 2: Average spectra and digital color histograms of different particle classes containing iron: a) fly ash, b) mineral dust, c) NaCl agglomerates, and d) Ca-S agglomerates. Average spectra are given as a relative area across the 19 elements analyzed by CCSEM-EDX (C, Na, Mg, Al, Si, P, S, Cl, K, Ca, Ti, Cr, Mn, Fe, Ni, Cu, Ni, Ba, and Pb). Digital color histogram heights represent the fraction of particles containing a specific element and colors represent the fraction containing specific ranges of intensities.

Figure 3: SEM images and EDX elemental maps of representative particles: a) fly ash, b) mineral dust, c) NaCl agglomerate, and d) Ca-S agglomerate. Elemental maps of Fe (red), O (green), Al (blue) or Si (aqua), and Na (orange) or Ca (pink), are shown for each class.

.

Figure 4: Circularity and aspect ratio of fly ash (green), mineral dust (brown), NaCl agglomerates (aqua), Ca-S agglomerates (orange), and other classes (gray) of iron-containing particles in a) summer 2008, b) summer 2009, and c) winter 2010.

Figure 5: Mass concentration by size of total particles (black line), fly ash (green), mineral dust (brown), NaCl agglomerates (aqua), Ca-S agglomerates (orange) in a) summer 2008, b) summer 2009, and c) winter 2010. Columns provide geographic segregation of size distributions with average across all sites (column 1), sites in the Cleveland Flats (column 2), Rest of Cleveland (column 3), and Medina (column 4). Inset upper right is a topographic map of the Cleveland area with different sites color coded by category: Flats (red), Rest of Cleveland (blue), Medina (green). For a detailed map of sources and sites in Cleveland see refs.[34,50,64] Note: Medina site was not used in 2008.

Figure 6: Circularity distributions for fly ash particles in a) summer 2008 and b) winter 2010 for the Cleveland Flats (solid line), Rest of Cleveland (dashed line), and Medina (2010 only, dotted line).

565 **Figure Captions**

566 Figure 1: Mass concentration by aerodynamic diameter of all particles (gray), iron-containing
567 particles (red), and the fraction of iron-containing particles (blue line) in a) summer 2008, b)
568 summer 2009, and c) winter 2010.

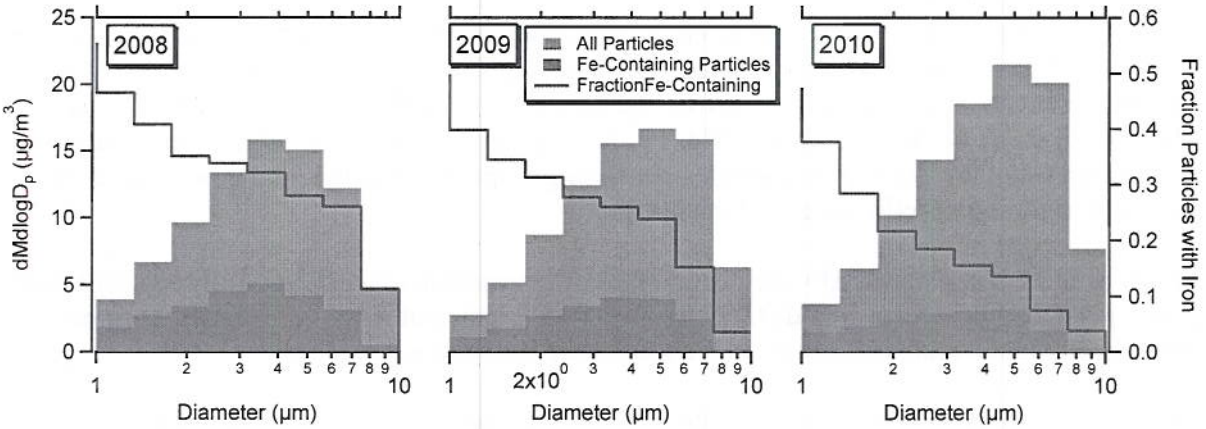

569
570
571

572 Figure 2: Average spectra and digital color histograms of different particle classes containing
573 iron: a) fly ash, b) mineral dust, c) NaCl agglomerates, and d) Ca-S agglomerates. Average
574 spectra are shown as relative x-ray peak areas across the 19 elements analyzed by CCSEM-EDX
575 (C, Na, Mg, Al, Si, P, S, Cl, K, Ca, Ti, Cr, Mn, Fe, Ni, Cu, Ni, Ba, and Pb). Digital color
576 histogram heights represent the fraction of particles containing a specific element and colors
577 represent the fraction containing specific ranges of intensities.

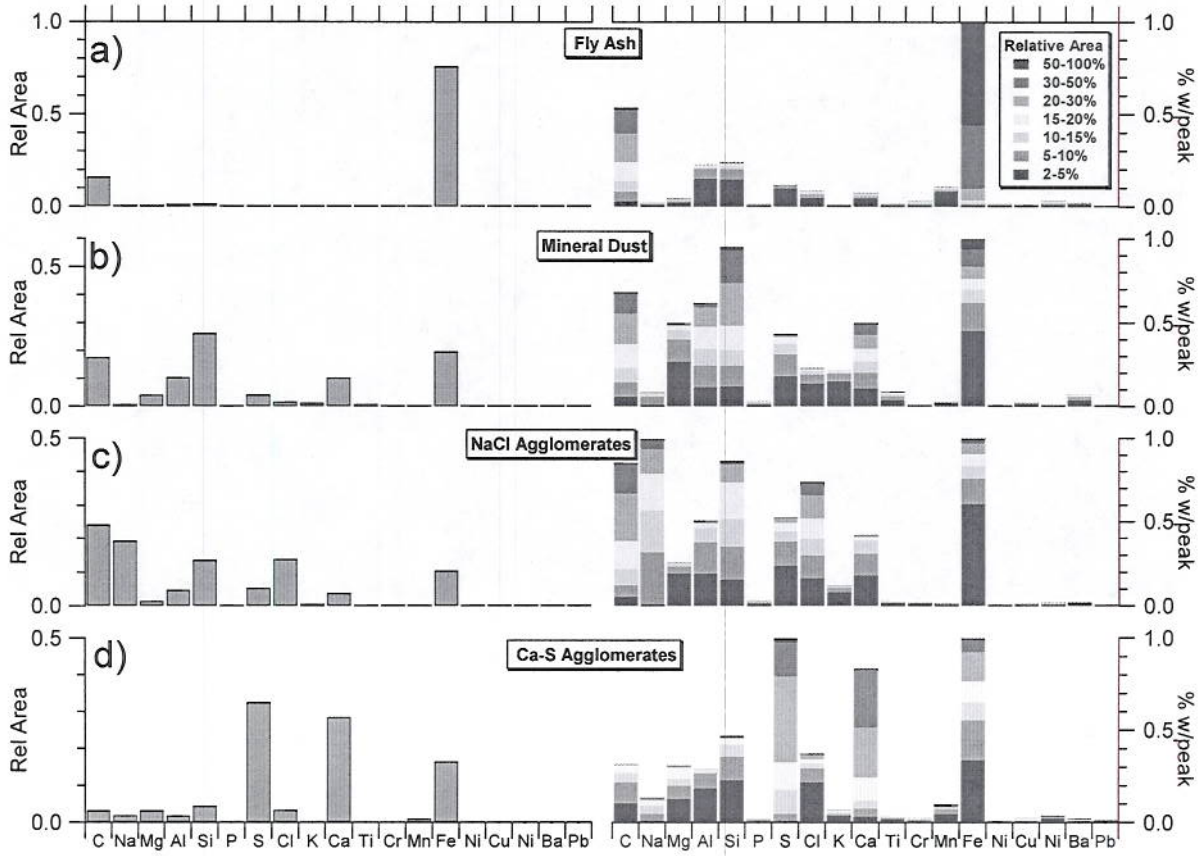

578

579 Figure 3: SEM images and EDX elemental maps of representative particles: a) fly ash, b) mineral
580 dust, c) NaCl agglomerate, and d) Ca-S agglomerate. Elemental maps of Fe (red), O (green), Al
581 (blue) or Si (aqua), and Na (orange) or Ca (pink), are shown for each class.

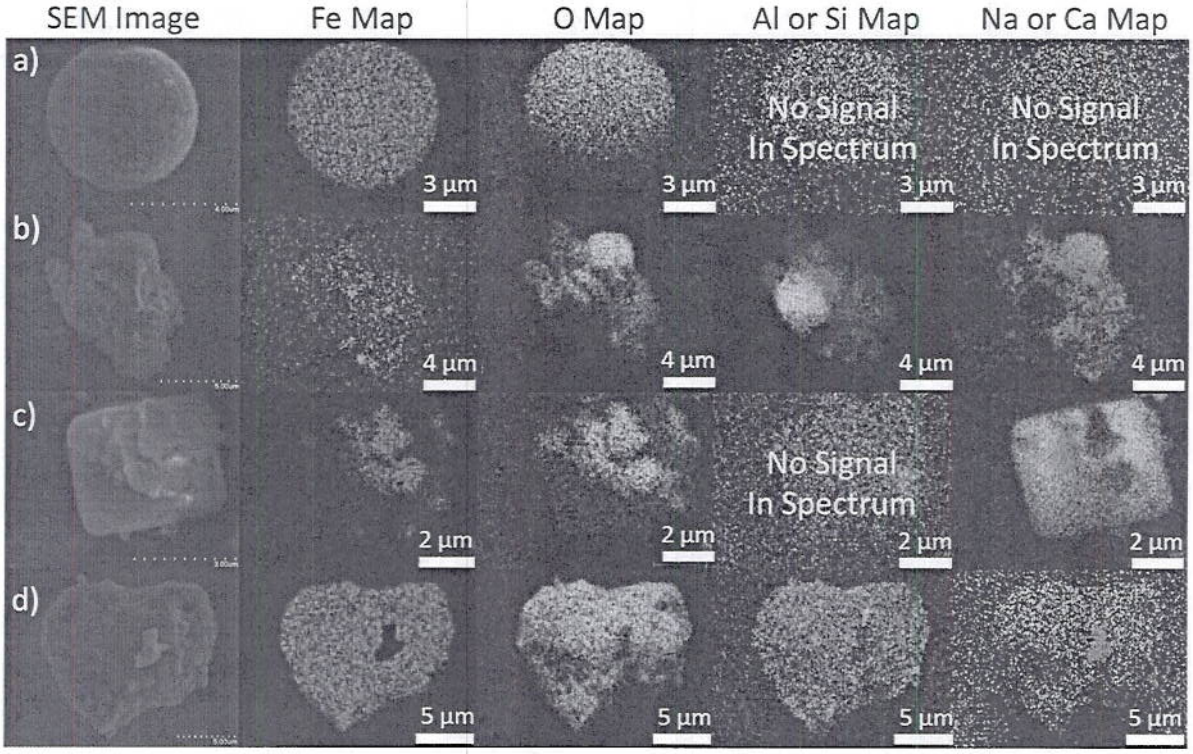

582

583

584

585 Figure 4: Circularity and aspect ratio of fly ash (green), mineral dust (brown), NaCl
586 agglomerates (aqua), Ca-S agglomerates (orange), and other classes of iron-containing particles
587 in a) summer 2008, b) summer 2009, and c) winter 2010.

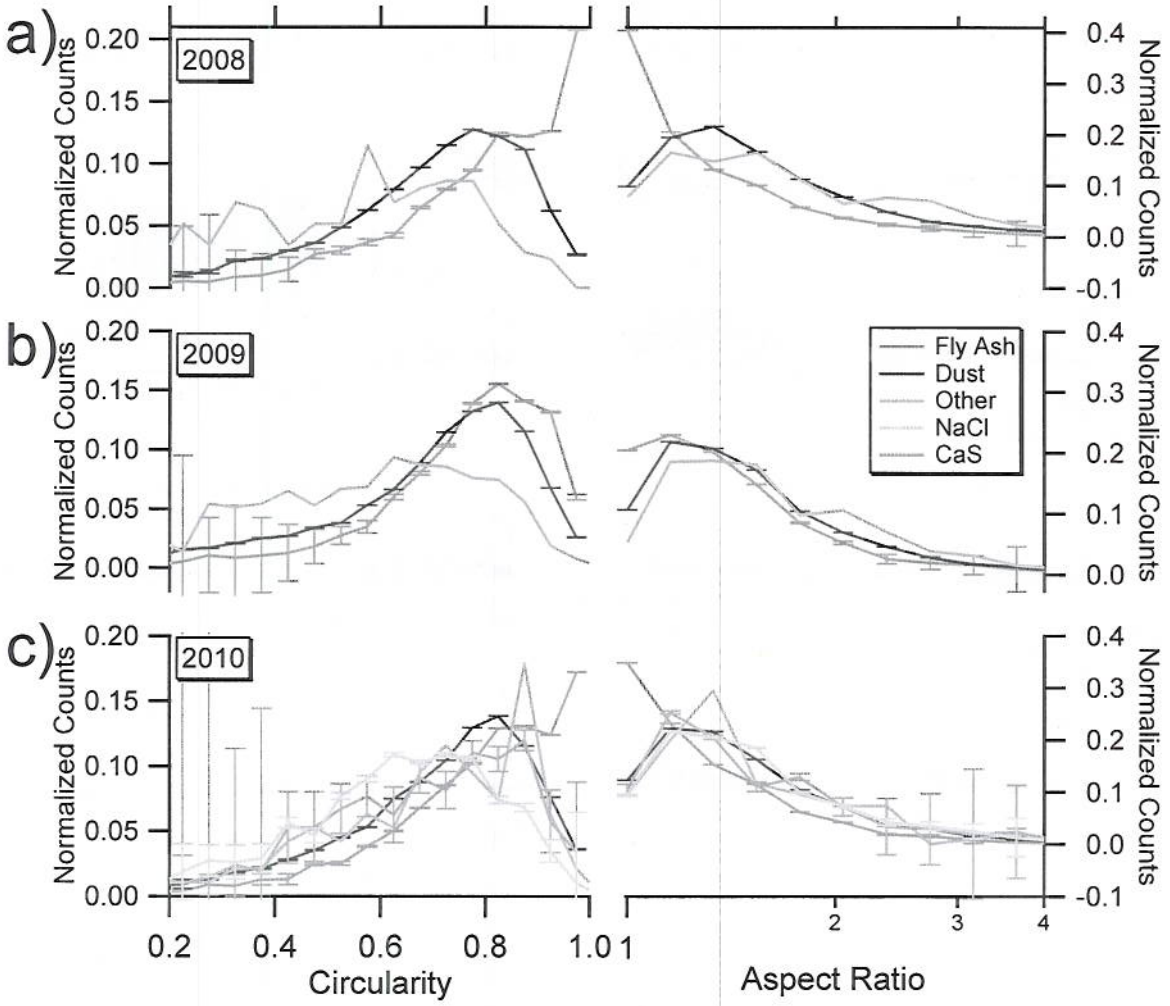

588

589 Figure 5: Mass concentration by size of total particles (black line), fly ash (green), mineral dust
590 (brown), NaCl agglomerates (aqua), Ca-S agglomerates (orange) in a) summer 2008, b) summer
591 2009, and c) winter 2010. Columns provide geographic segregation of size distributions with
592 average across all sites (column 1), sites in the Cleveland Flats (column 2), Rest of Cleveland
593 (column 3), and Medina (column 4). Inset upper right is a topographic map of the Cleveland area
594 with different sites color coded by category: Flats (red), Rest of Cleveland (blue), Medina
595 (green). For a detailed map of sources and sites in Cleveland see refs.[34,50,64] Note: Medina site
596 was not used in 2008.

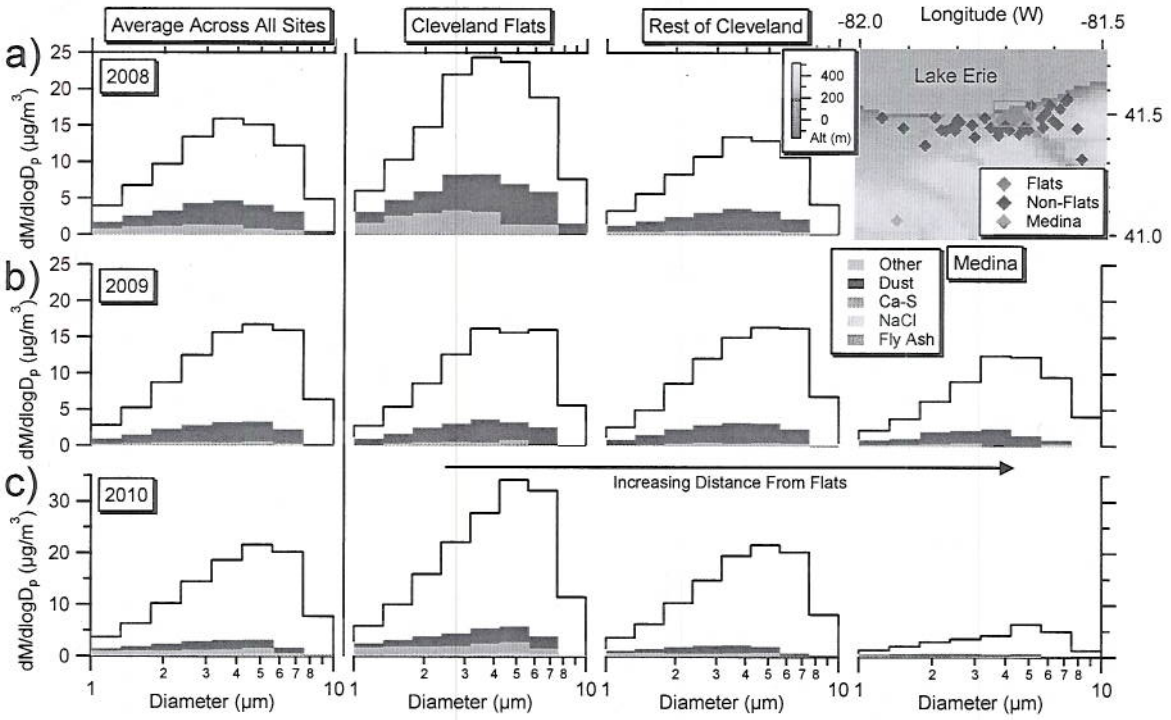

597

598 Figure 6: Circularity distributions for fly ash particles in a) summer 2008 and b) winter 2010 for
599 the Cleveland Flats (solid line), Rest of Cleveland (dashed line), and Medina (2010 only, dotted
600 line).

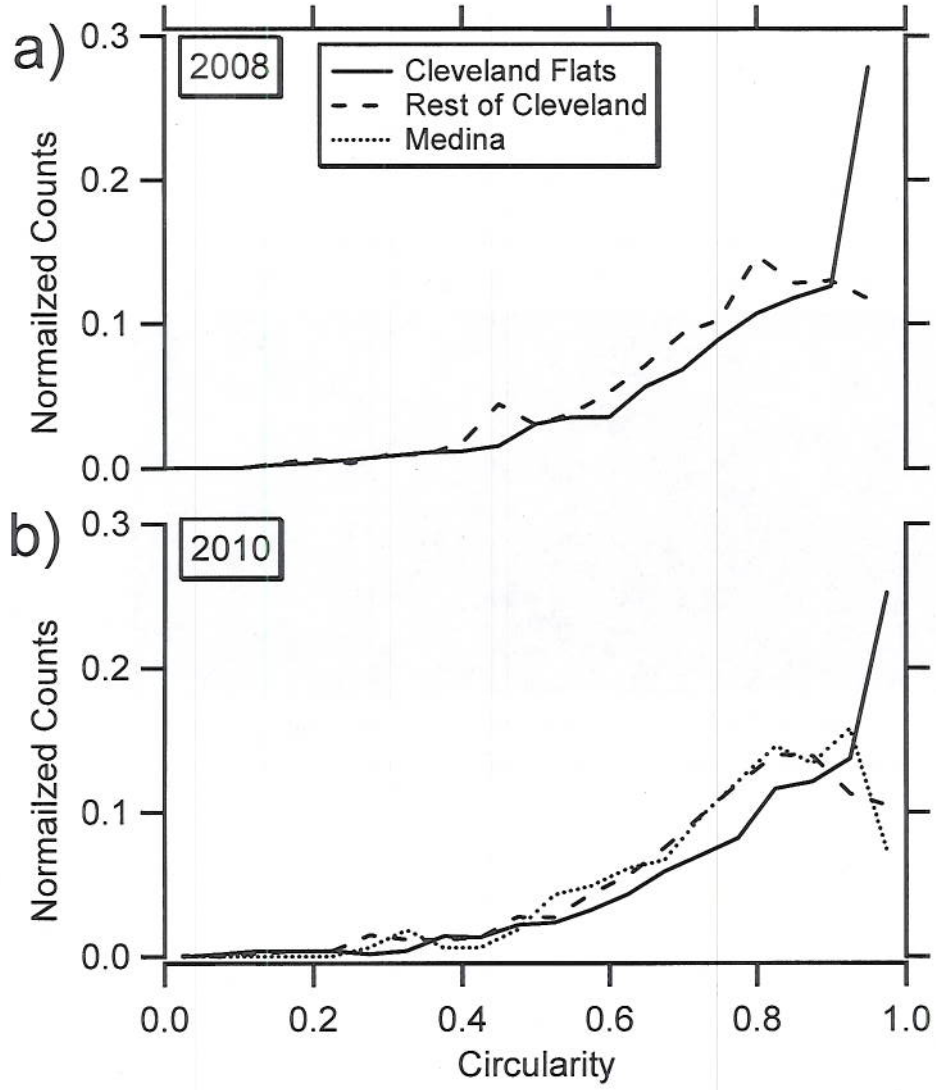

601

602

603 **Brief:**

604 Sources, spatial distribution, and atmospheric processing of natural and anthropogenic iron-
605 containing particles are shown for the Cleveland, Ohio urban airshed.

606

607 **TOC – Graphic**

608

609

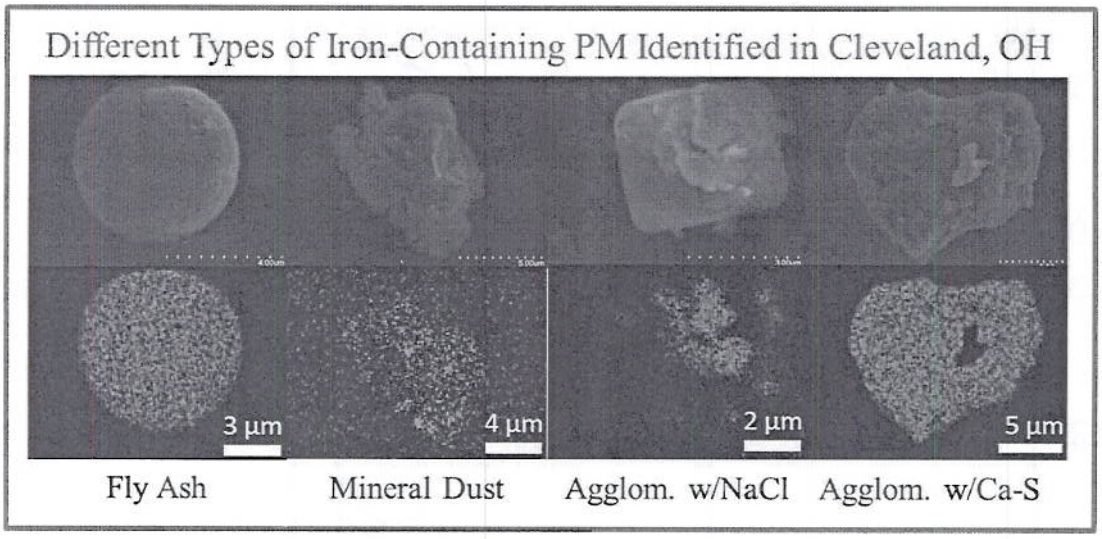

610